Chalcogenide Letters Vol. 11, No. 10, October 2014, p. 471 - 484

# ELASTIC AND STRUCTURAL PROPERTIES OF (95-$x$)$TeO_2$-5$La_2O_3$-$x$$TiO_2$ LANTHANUM TELLURITE GLASS SYSTEM

I.N. SAPIAN, M.I.M.YUSOF, A.K.YAHYA*
*Faculty of Applied Sciences, Universiti Teknologi Mara,40450 Shah Alam, Selangor, Malaysia*

Lanthanum tellurite (95-$x$)$TeO_2$-5$La_2O_3$-$x$$TiO_2$, ($x$ = 0 - 20 mol%) glasses were prepared by the melt-quenching method. Elastic and structural properties of the glasses were studied by measuring sound velocity using the pulse-echo-overlap technique and Fourier Transform Infrared (FTIR) spectroscopy, respectively. In addition, the glass transition temperature, $T_g$ was investigated using Differential Scanning Calorimetry (DSC) measurements. Both independent moduli ($C_L$ and $\mu$) and related elastic moduli such as bulk modulus ($K_e$), Young's modulus ($E$), hardness ($H$) and Debye temperature ($\theta_D$) were observed to increase gradually for $x$ < 15 mol% followed by a large increase at $x$ = 20 mol% addition of $TiO_2$. The results obtained showed that this glass system becomes more stable, rigid and stiffer with addition of $TiO_2$. Structural analysis showed increase in bridging-oxygen (BO) compared to non-bridging oxygen (NBO). $T_g$ increased with addition of $TiO_2$ and confirms the increasing rigidity of the network. Theoretical analysis using bulk compression and ring deformation models showed a gradual increase in ratio of ideal bulk modulus compared to experimental bulk modulus, $K_{bc}/K_e$ for $x$ < 15 mol% before a sudden drop at $x$ = 20 mol%. The drop indicates decrease in ring deformation or bending. Although some deformation or bending may take place during compression, the main compression mechanism was still mainly isotropic ring compression.

(Received August 7, 2014; Accepted October 1, 2014)

*Keywords*: Elastic properties; FTIR; Lanthanum tellurite glass; Ultrasonics

## 1. Introduction

Tellurium oxide ($TeO_2$) based glasses also known as tellurite glass have gained strong interest among researchers due to their physical properties that possesses high dielectric constant [1-3], high refractive index [4, 5], good infrared transmission [6, 7], good mechanical strength [8, 9] and low hygroscopic properties [10] compared to phosphate ($P_2O_5$) and borate ($B_2O_3$) glasses. These properties allow tellurite glasses to be used in developing new glasses for many technological applications such as in optical switches [11], ultraviolet-induced photo-refractive gratings [12] and optical fiber amplifiers [13]. $TeO_2$ is a conditional glass former which do not form glasses by themselves, but acts like glass formers when combined with other modifier such as heavy metal, alkali, alkaline earth or transition metal oxides [14-17].

Several studies have been reported on structural [18, 19], optical [20, 21], and thermal [18, 22] properties of binary, ternary and quaternary titanate-tellurite glass systems. Previous study on structural properties of binary (100-$x$)$TeO_2$-$x$$TiO_2$ glass system by Raman spectra show that as $TiO_2$ content is increased, the Te-O-Te linkage are dynamically changed by formation of Ti-O-Ti linkage which strengthens the network structure [18]. Interestingly for ternary 0.8$TeO_2$-(0.2-$x$)BaO-$x$$TiO_2$, it was reported that non-linear coefficent such as refractive index, $n$ and non-linear optical absorption, $\beta$ are larger than other $TiO_2$-containing phosphate, borophosphate glasses [23] or other tellurium oxide glasses [24, 25]. The study also shows that the addition of $TiO_2$ develops additional formation of covalent bonds and favours a continuous network consisting of distorted $TiO_6$ unit indicating increased number of bridging oxygen (BO). On the other hand, interestingly,

*Corresponding author: ahmad191@salam.uitm.edu.my

addition of rare-earth oxide such as $La_2O_3$ to tellurite glass increases stability of the glasses against crystallization [26]. Other study also show that $La_2O_3$ doped tellurite glass showed higher $T_g$, $\Delta T$ and glass viscosity compared with the base glass and is of benefit for fiber fabrication [27].

On the other hand, ultrasonic velocity measurement technique is a useful tool for studies on elastic properties of glasses. Independent elastic moduli can be computed from longitudinal and shear velocity and density data to give information on strength, rigidity [15-17], stiffness [10, 28, 29] and other elastic moduli of the glasses. A number of studies have shown that rigidity and elastic constant of the glasses changes considerably with transition metal oxide doping in tellurite glass systems. In addition, it is interesting to study elastic properties together with the study of structural properties as modification of glass network involving formation of number of bridging oxygen (BO) increased rigidity and stiffness of glass. While the increase in non-bridging oxygen (NBO) has a reverse effect. Previous study on quaternary $47P_2O_5$-30.5CaO-(22.5-$x$)$Na_2O$-$x$$TiO_2$ glass [30] reported that ultrasonic velocity decreased for x = 0 – 0.5 mol% due to conversion of BO into NBO but further addition of $TiO_2$ (x > 0.5 mol%) showed increase in ultrasonic velocity and elastic moduli with formation of BO.

Interestingly, previous study on ternary $50TeO_2$-$50V_2O_5$-$x$$TiO_2$ glass system [14] showed that the increase in longitudinal modulus, $C_L$, shear modulus, $C_s$, bulk modulus, $K$ and Young's modulus, $Y$ with addition of $TiO_2$ is attributed to increase in the rigidity of the glass. In addition, the bulk modulus of the ternary glass was reportedly higher than that reported for binary $TeO_2$–$V_2O_5$ [31]. Quiet recently, studies on thermal properties of (95-$x$)$TeO_2$-$5La_2O_3$-$x$$TiO_2$ lanthanum tellurite glass system have been reported to show increase in glass transition, $T_g$, onset crystallization temperature, $T_x$ and improvement in thermal stability factor $\Delta T = T_x - T_g$ for $0 \leq x \leq$ 20 mol% of $TiO_2$ [22]. Thus, for $TeO_2$-$La_2O_3$-$TiO_2$ glass, it is expected that longitudinal modulus, $C_L$, shear modulus, $C_S$ and also other moduli such as Young's modulus, $E$ and bulk modulus, $K$ are modified due to presence of both $La_2O_3$ and $TiO_2$ in the tellurite system. However, to our knowledge, the study of elastic properties in concurrence with the study on structural properties of (95-$x$)$TeO_2$-$5La_2O_3$-$x$$TiO_2$ glass has not been previously reported.

The purpose our present work is to investigate the influence of glass network modification by $TiO_2$ addition in (95-$x$)$TeO_2$-$5La_2O_3$-$x$$TiO_2$ ($x$ = 0, 5, 10, 15 and 20 mol %) glass system on elastic and structural properties of the glasses. At the same time, the correlation between ultrasonic velocity measurements and FTIR spectroscopy were performed together to correlate the structure modification of glass network with the elastic properties. In addition, effect of $TiO_2$ addition on bulk modulus, $K$ was analyzed and discussed using the bulk compression and ring deformation models.

## 2. Experimental Details

### 2.1 Samples preparation

The ternary (95-$x$)$TeO_2$-$5La_2O_3$-$x$$TiO_2$ glass system with $x$ = 0, 5, 10, 15 and 20 mol% were prepared using conventional solid state method and melt-quenching technique. The powder of $La_2O_3$, $TiO_2$ and $TeO_2$ with purity > 99.99% was mixed and ground in an agate mortar in an hour to reach homogeneous and fined grained mixture. The mixed batches were then melted at 900°C in an hour. The melt was quickly quenched by pouring it on stainless steel plate before annealed at 200°C for 2 hours. The glasses were then grounded into powder to meet the requirement of X-ray diffraction (XRD), glass transition temperature ($T_g$) and Infrared (IR) absorption measurement.

### 2.2Characterization of samples

XRD analysis was performed to confirm the amorphous nature of the glass samples by using X'Pert Pro Panalytical diffractometer. $T_g$ was determined by differential scanning calorimetry using NETZSCH model DSC 200 F3 at a heating rate of 10 ˚C/min. IR absorption analysis.was performed in the region of 400-1000 $cm^{-1}$ with NICOLET model 560 spectrometer,

using KBr pellets at room temperature. The density, $\rho$ of the glass samples were determined using Archimedes principle with xylene as an immersion medium using the relation.

$$\rho = \left( \frac{Wa}{Wa - Wb} \right) \rho_b \tag{1}$$

where $W_a$ is the glass sample weight in air, $W_b$ is the glass sample weight in water and $\rho_b$ is the density of xylene (0.865 g/mL). The samples were polished using fine sand paper to obtain parallel opposite faces as required for ultrasonic velocity measurement. Ultrasonic velocity measurements were measured in both longitudinal and shear modes at room temperature by applying the pulse echo-overlap technique at 5MHz using Matec model 7700system. The related elastic moduli were calculated using the equations [16, 17, 32-34]:

Longitudinal modulus, $C_L = v_L^2 \rho$ (2)

Shear modulus, $\mu = v_s^2 \rho$ (3)

Bulk modulus, $K_e = C_L - \left( \frac{4}{3} \right) \mu$ (4)

Young's modulus, $Y = \frac{9K\mu}{3K + \mu}$ (5)

Hardness, $H = \frac{(1 - 2\sigma)Y}{6(1 + \sigma)}$ (6)

Poisson's ratio, $\sigma = \frac{C_L - 2\mu}{2(C_L - \mu)}$ (7)

Debye temperature, $\theta_D = \left( \frac{h}{k_B} \right) \left( \frac{3PN_A}{4\pi V_a} \right)^{1/3} v_m$ (8)

where $h$ is the Planck's constant, $k_B$ is the Boltzmann's constant, $N_A$ is the Avogadro number, $V_a$ is the molar atomic volume calculated from the effective molecular mass and the density ($M/\rho$), $P$ is the number of atoms in the chemical formula and $v_m$ is the mean sound velocity defined by the relation:

$$v_m = \left[ \frac{3v_L^3 v_s^3}{v_L^3 + v_s^3} \right]^{1/3} \tag{9}$$

Further analysis of the result of elastic measurements has been performed using the bulk compression and the ring deformation models**.** In the bulk compression model, it assumed that the compression is isotropic in all directions with change in bond length without accompaning change in bond angles [35]. The theoretical bulk modulus, $K_{bc}$ for polycomponent glasses with $n$ different types of network bonds can be computed using [35] :

$$K_{bc} = \frac{N_A}{9V_a} \sum \left( x n_f r^2 F \right)_n \tag{10}$$

where $N_A$ is Avogadro number, $x$ is the mole fraction of the component oxide $i$, $n_f$ is the coordination number of cation, $r$ is the bond length, $F$ is the stretching force constant of oxide, $n$ is the mole fraction of component oxide. The ring size, $l$ is calculated by the relation derived from the ring deformation model [36]:

$$l = [0.0106 \frac{\overline{F}_a}{K_e}]^{0.26} \tag{11}$$

where $K_e$ is the experimental bulk modulus, $\overline{F}_a$ is the average stretching force constant of glass and it is calculated using equation [36]:

$$\overline{F}_a = \frac{\sum (x n_f F)_n}{\sum (x n_f)_n} \tag{12}$$

The average ideal cross-link density, $\overline{n}_c$ was calculated by equation [35]:

$$\overline{n}_c = \frac{1}{\eta} \sum_i (n_c N_c) \tag{13}$$

where $n_c$ is number of bridging bonds per cation minus two , $N_c$ is number of cations per glass formula unit and $\eta$ is total number of cations per glass formula unit.

## 3. Result and analysis

The XRD patterns for all samples of the (95-$x$)$TeO_2$-5$La_2O_3$-$x$$TiO_2$($x$ = 0 - 20 mol %) glass system showed no crystalline peak confirming the amorphous nature of the samples (Fig. 1). Table 1 gives the values of density ($\rho$), molar volume ($V_a$), longitudinal velocity ($v_L$), shear velocity ($v_s$) and mean velocity ($v_m$) for all samples. Fig. 2 shows the variation of $\rho$ and $V_a$ with $TiO_2$ content for the (95-$x$)$TeO_2$-5$La_2O_3$-$x$$TiO_2$ glass system. From the figure it can be seen that the value of $\rho$ gradually decreases with addition of $TiO_2$ content from 5557kgm$^{-1}$ ($x$=0 mol %) to 5382 kg m$^{-1}$ ($x$=20 mol %). Meanwhile, as $TiO_2$ increased, the molar volume, ($V_a$) of the glasses also steadily decreased from 3.02m$^3$ mol $^{-1}$($x$ = 0 mol %) to 2.82 m$^3$ mol$^{-1}$($x$ = 20 mol %).

Fig. 3 shows the infrared (IR) absorption spectra for the (95-$x$)$TeO_2$-5$La_2O_3$-$x$$TiO_2$ ($x$ = 0, 5, 10, 15 and 20 mol %) glasses in the frequency range from 500-1000 cm$^{-1}$ at room temperature. Fig.4 shows the deconvolution of IR absorption spectrum for the $x$ = 0 mol% and $x$ = 5 mol% of glass samples. Four major IR absorption bands observed in Fig. 3 were at ~547, ~659, ~780 and ~864 cm$^{-1}$. The ~547 cm$^{-1}$ IR peak is assigned to $TeO_{3+1}$ while the ~659 cm$^{-1}$ peak is assigned to $TeO_4$ trigonal bipyramid (tbp) group [16]. The IR frequency peaks at ~780 $^{-1}$ and ~864 cm$^{-1}$ are assigned to $TeO_3$ trigonal pyramid (tp) group [16, 34] and streching vibrations of $TiO_4$ [22], respectively. The ~864 cm$^{-1}$ band was observed to increase from 844 cm$^{-1}$ ($x$ = 5 mol %) to 866 cm$^{-1}$ ($x$ = 20 mol %).

The DSC curves for $0 \leq x \leq 20$ mol% of $TiO_2$ are shown in Fig. 5. The values of glass transition temperature ($T_g$), onset crystallization temperature, ($T_o$), temperature of the first crystallization peak ($T_x$) and thermal stability, ($\Delta T = T_o - T_g$) are tabulated in Table 2. The values of $T_g$ which were determined at the DCS curve (Fig. 5) increases from 338˚C ($x$ = 0 mol%) to 404˚C ($x$ = 20 mol%) with addition of $TiO_2$. The calculated values of $\Delta T$ showe dincrease from 37˚C ($x$ = 0 mol%) to 127˚C ($x$ = 20 mol%) with addition of $TiO_2$ content.

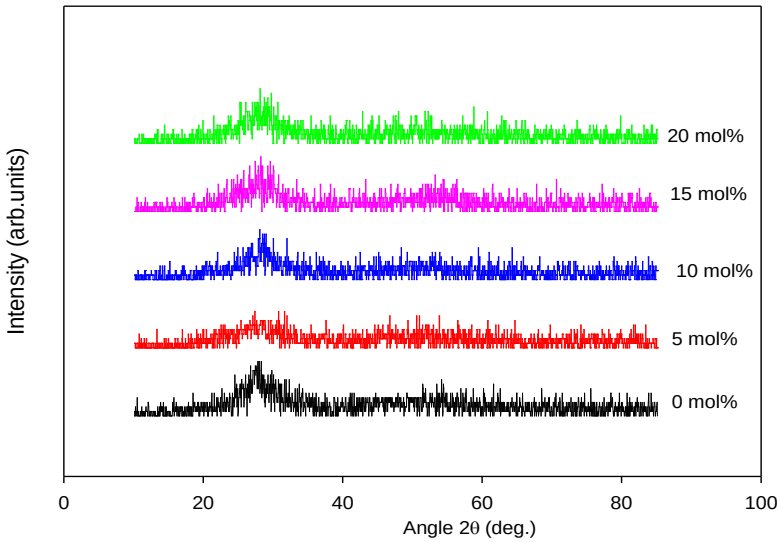


*Fig.1. XRD pattern of (95-x)$TeO_2$-5$La_2O_3$-x$TiO_2$ (x = 0, 5, 10, 15 and 20 mol %) glass system*

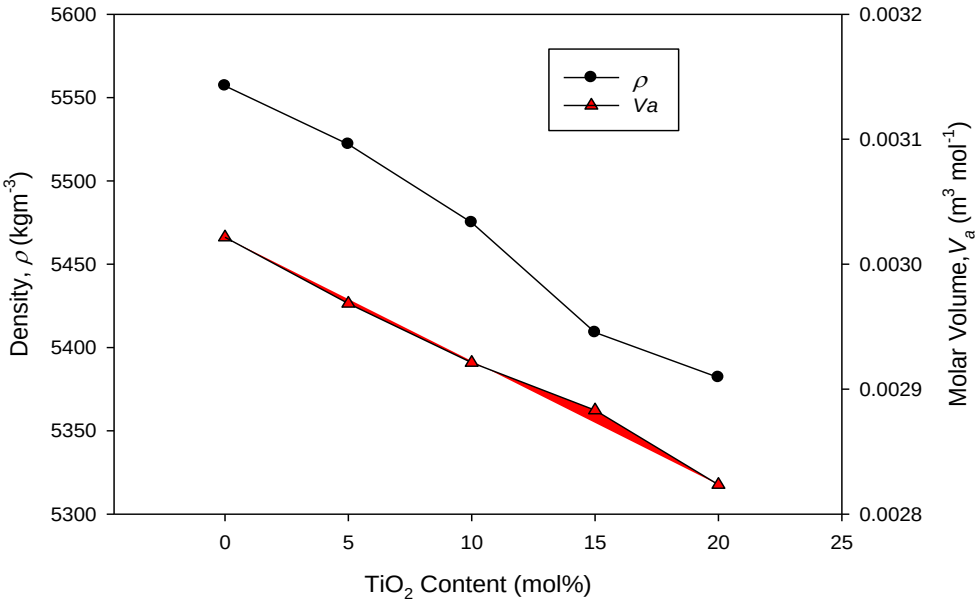


*Fig.2: Density, ρ and molar volume, $V_a$ of (95-x)$TeO_2$-5$La_2O_3$-x$TiO_2$ (x = 0, 5, 10, 15 and 20 mol %) glass system*

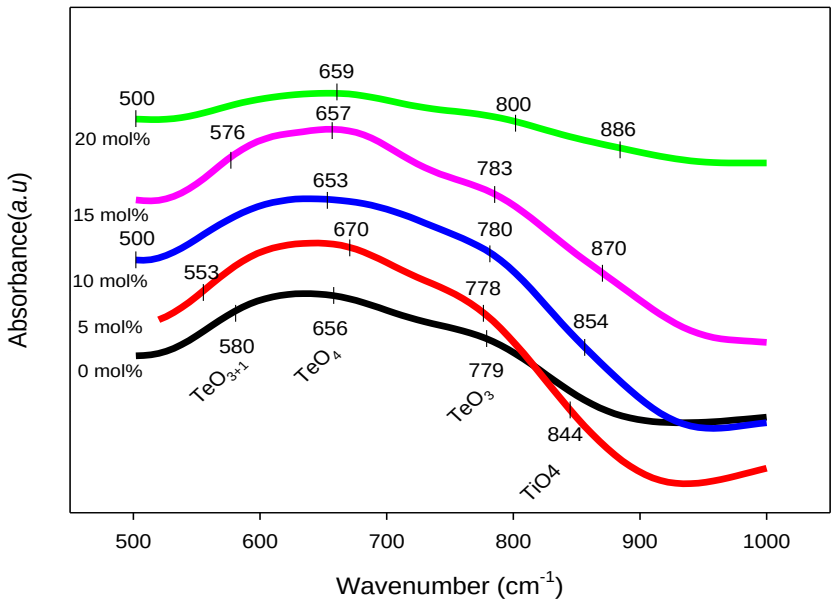


*Fig. 3: IR spectra of (95-x)$TeO_2$-5$La_2O_3$-x$TiO_2$ (x = 0, 5, 10, 15 and 20 mol %) glass system*

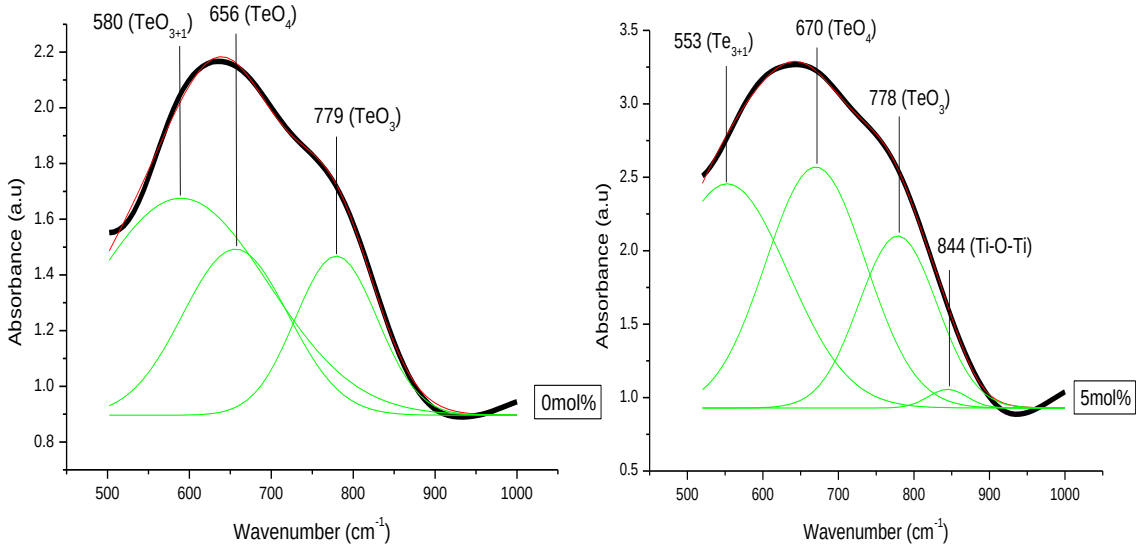


*Fig. 4. Deconvoluted FTIR spectra of (95-x)$TeO_2$-5$La_2O_3$-x$TiO_2$ (x = 0 and 5 mol %) glass system using a Gaussian type function*

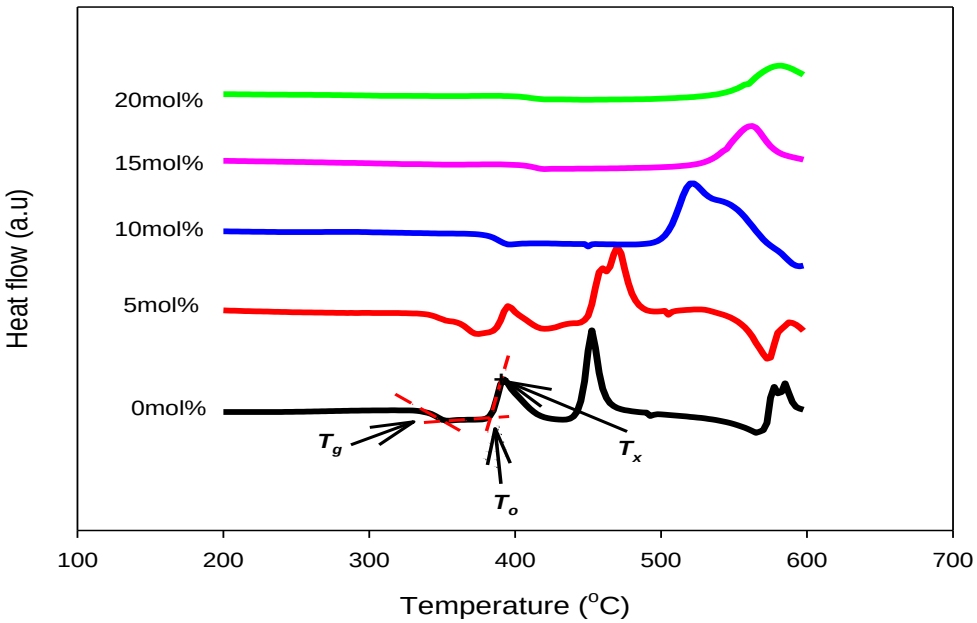


*Fig. 5. DSC curves of (95-x)$TeO_2$-5$La_2O_3$-x$TiO_2$ (x = 0, 5, 10, 15 and 20 mol %) glass system*

*Table1.Values of density (ρ), molar volume ($V_a$), longitudinal velocity ($v_L$), shear velocity ($v_s$) and mean velocity ($v_m$) of (95-x)$TeO_2$-5$La_2O_3$-x$TiO_2$ glass system*

| **x (mol %)** | **ρ (kg $m^{-3}$) ±7** | **$V_a$ ($m^3$/mol) x $10^{-3}$** | **$v_L$ (km $s^{-1}$) ±0.01** | **$v_s$ (km $s^{-1}$) ±0.01** | **$v_m$ (km $s^{-1}$) ±0.01** |
|---|---|---|---|---|---|
| **0** | 5557 | 3.02 | 3.13 | 1.57 | 2.10 |
| **5** | 5522 | 2.97 | 3.20 | 1.65 | 2.19 |
| **10** | 5475 | 2.92 | 3.40 | 1.87 | 2.45 |
| **15** | 5409 | 2.88 | 3.52 | 1.99 | 2.59 |
| **20** | 5382 | 2.82 | 3.97 | 2.45 | 3.11 |

*Table 2.Values of temperature glass transition temperature ($T_g$), onset crystallization temperature, ($T_o$), temperature of the first crystallization peak ($T_x$) and thermal stability, (ΔT) of (95-x)$TeO_2$-5$La_2O_3$-x$TiO_2$ glass system.*

| **x (mol%)** | **$T_g$ (°C)** | **$T_o$ (°C)** | **$T_x$ (°C)** | **$\Delta T = T_o - T_g$ (°C)** |
|---|---|---|---|---|
| **0** | 338 | 375 | 392 | 37 |
| **5** | 347 | 386 | 395 | 39 |
| **10** | 381 | 493 | 521 | 112 |
| **15** | 402 | 520 | 562 | 118 |
| **20** | 404 | 531 | 581 | 127 |

Fig. 6 shows the longitudinal velocity, $v_L$ and shear velocity, $v_s$ for the (95-x)$TeO_2$-5$La_2O_3$-x$TiO_2$ (x = 0-20 mol %) glass system. Both $v_L$ and $v_S$ increased for $x$ < 15 mol % from 3.13 km $s^{-1}$ ($x$ = 0 mol %) to 3.52 km $s^{-1}$ ($x$ = 15 mol %) and from 1.57 km $s^{-1}$ ($x$ = 0 mol %) to 1.99 km $s^{-1}$ ($x$ = 15 mol %), respectively followed by a large increase at $x$ = 20 mol % with 3.97 km $s^{-1}$ ($v_L$) and 2.45 km $s^{-1}$ ($v_S$).

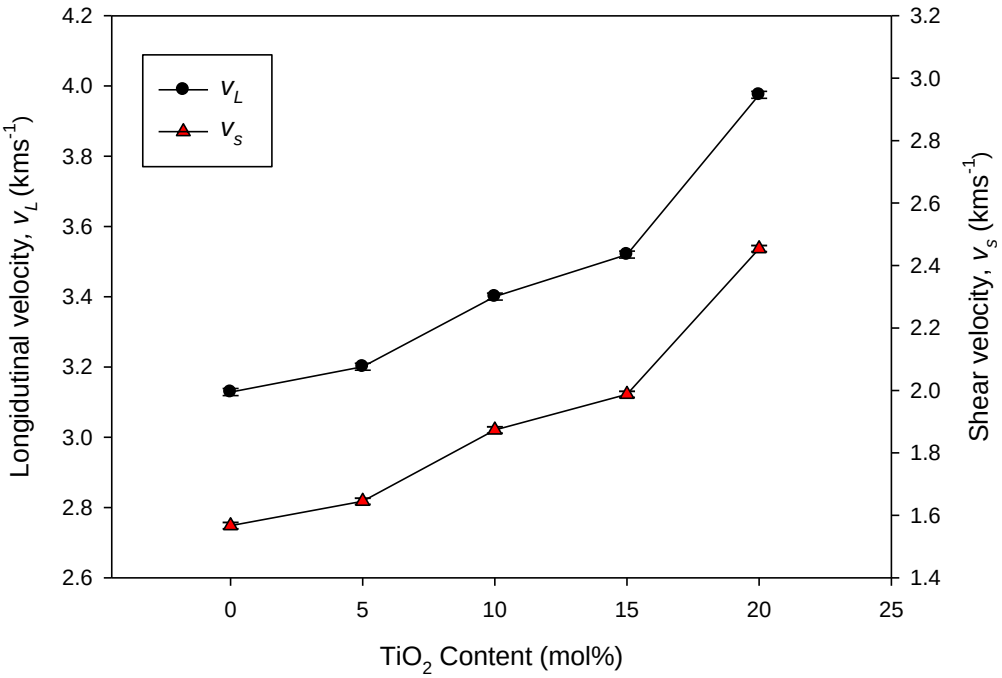


*Fig.6: Longitudinal velocity, $v_L$ and shear velocity, $v_s$ of (95-x)$TeO_2$-5$La_2O_3$-x$TiO_2$ (x = 0, 5, 10, 15 and 20 mol %) glass system*

Table 3 represents the calculated values of longitudinal modulus ($C_L$), shear modulus ($\mu$), bulk modulus ($K_e$), Young's modulus ($E$), hardness ($H$), Poisson's ratio ($\sigma$) and Debye temperature ($\theta_D$) by using Eqs. (2) to (8). Longitudinal modulus ($C_L$) and shear modulus ($\mu$) also increased as addition of $TiO_2$ increased and show similar trend with $v_L$ and $v_s$ (Fig. 7). Meanwhile, the behaviours of bulk modulus ($K_e$) and Young's modulus ($E$) with addition of $TiO_2$ content are showed in Fig. 8. The behaviours of $K_e$ and $E$ were generally similar to the behaviours of the independent moduli ($C_L$ and $\mu$) as shown in Fig. 7. Both $K_e$ and $E$ showed generally steady increased from $x$ = 0 to 15 mol% followed by slightly larger increase for $x$ > 15 mol % (Table 3). On the other hand, Poisson's ratio ($\sigma$) decreases linearly from 0.33($x$ = 0 mol%) to 0.27 ($x$ = 15 mol%) before a larger decrease to 0.19 ($x$ = 20 mol%). In contrast hardness ($H$) increases linearly from 1.5 GPa ($x$ = 0 mol%) to 3.3 GPa ($x$ = 15 mol%) before a larger increase to 6.7 GPa ($x$ = 20 mol%) (Fig. 9). Fig. 10 showed the behavior of the Debye temperature ($\theta_D$) and mean velocity, $v_m$. Both $\theta_D$ and $v_m$also showed quite similar trends to the independent moduli ($C_L$ and $\mu$).

*Table 3.Values of longitudinal modulus ($C_L$), shear modulus ($\mu$), bulk modulus ($K_e$), Young's modulus (E), hardness (H), Poisson's ratio ($\sigma$) and Debye temperature ($\theta_D$) of (95-x)$TeO_2$-5$La_2O_3$-x$TiO_2$ glass system.*

| **x (mol %)** | **$C_L$ (GPa) ±0.5** | **$\mu$ (GPa) ±0.3** | **$K_e$(GPa) ±0.8** | **$E$(GPa) ±3** | **$H$(GPa) ±0.4** | **$\sigma$ ±0.01** | **$\theta_D$ (GPa) ±5** |
|---|---|---|---|---|---|---|---|
| **0** | 54.4 | 13.6 | 36.2 | 36.4 | 1.5 | 0.33 | 247 |
| **5** | 56.6 | 14.9 | 36.6 | 39.5 | 1.9 | 0.32 | 259 |
| **10** | 63.3 | 19.2 | 37.6 | 49.3 | 2.8 | 0.28 | 292 |
| **15** | 67.0 | 21.4 | 38.5 | 54.1 | 3.3 | 0.27 | 309 |
| **20** | 85.0 | 32.4 | 41.8 | 77.3 | 6.7 | 0.19 | 375 |

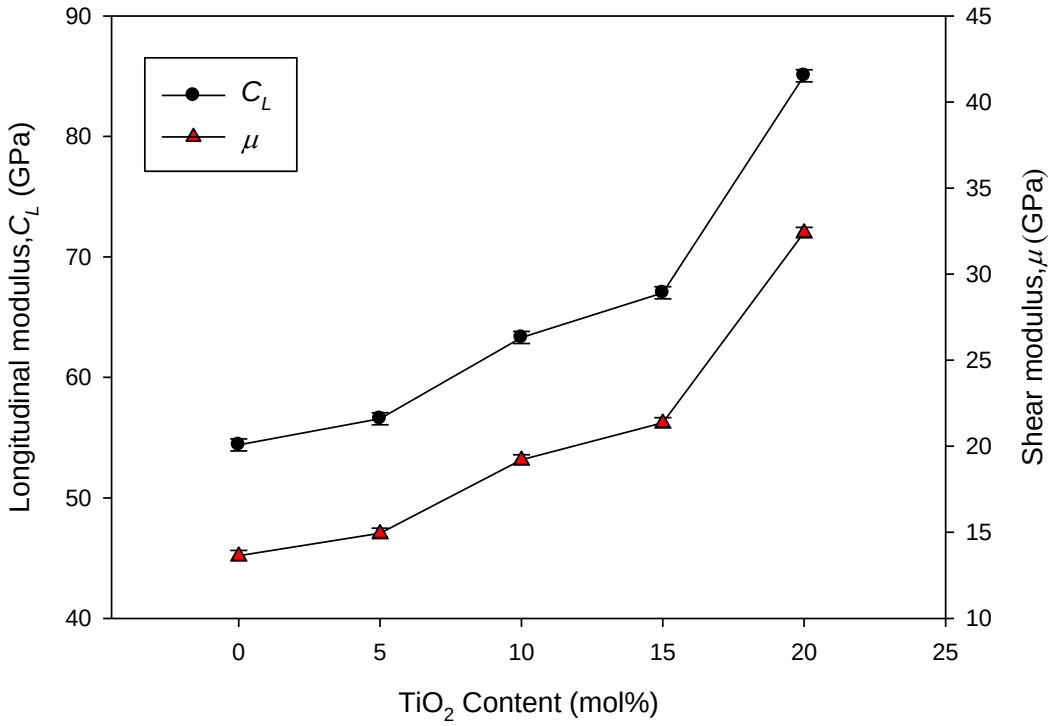


*Fig.7.: Longitudinal modulus, $C_L$ and shear modulus, $\mu$ of (95-x)$TeO_2$-5$La_2O_3$-x$TiO_2$ (x = 0, 5, 10, 15 and 20 mol %) glass system*

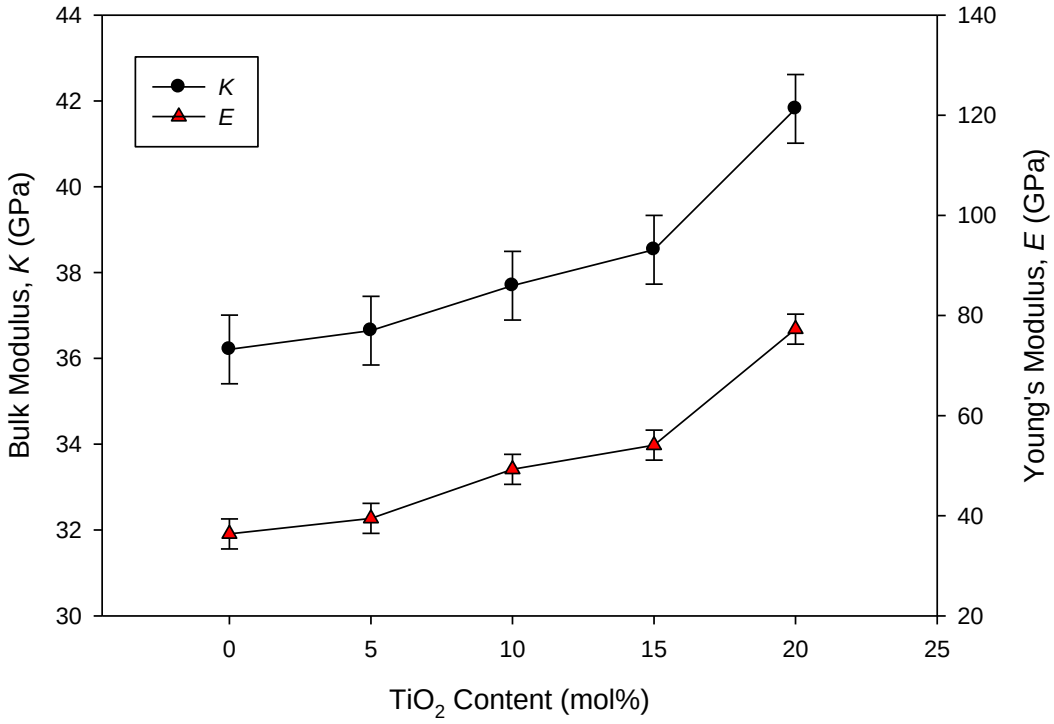


*Fig.8. Bulk modulus, $K_e$ and Young's modulus, E of (95-x)$TeO_2$-5$La_2O_3$-x$TiO_2$ glass system*

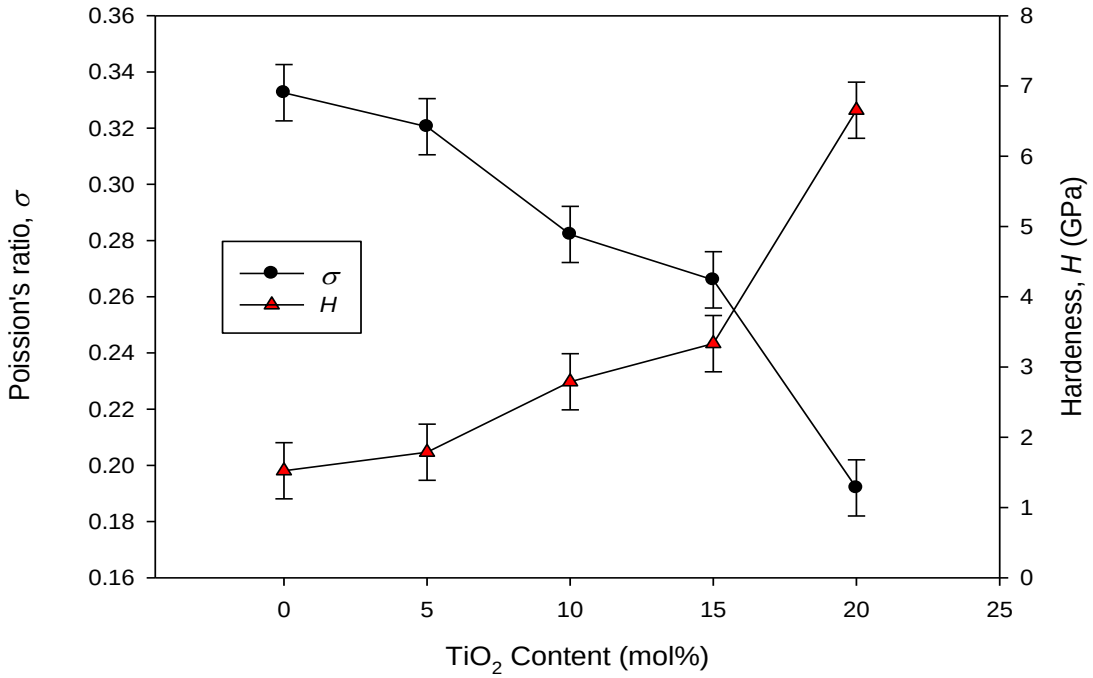


*Fig.9..Hardness, H and Poisson's Ratio, σ of (95-x)$TeO_2$-5$La_2O_3$-x$TiO_2$ glass system*

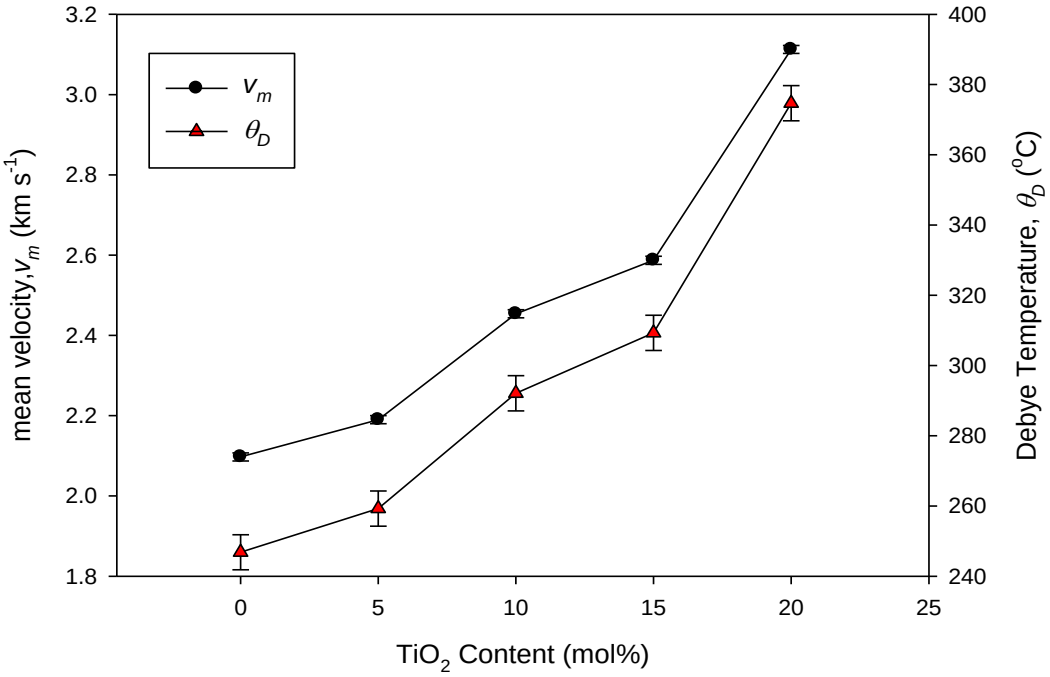


*Fig. 10. Debye temperature, $\theta_D$ and mean velocity, $v_m$ of (95-x)$TeO_2$-5$La_2O_3$-x$TiO_2$ glass system*

Table 4 represents the values of coordination number ($n_f$), crosslink density per cation ($n_c$), cation–anion bond length ($r$), and stretching force constant ($F$) of the oxides of $TeO_2$, $La_2O_3$ and $TiO_2$. Table 5 represents the values of bulk modulus ($K_{bc}$), ratio of ($K_{bc}/K_e$), number of bonds per unit volume ($n_b$), and average stretching force constant ($F$). The calculated ideal average crosslink density, $n_c$ as given in Table 4, increase linearly with $TiO_2$ content. The relation between $K_{bc}/K_e$

and the calculated average ring size, $l$ is inversely proportional with $TiO_2$ addition up to 15mol% but at $x$ = 20 mol%, $K_{bc}/K_e$ as well as $l$ decreased (Fig. 11).

*Table 4. Values of coordination number ($n_f$), crosslink density per cation ($n_c$), cation–anion bond length (r), and stretching force constant (F) of the oxides of $TeO_2$, $La_2O_3$ and $TiO_2$.*

| Oxide | $n_f$ | $n_c$ | $r$ (nm) | $F$ (N m$^{-1}$) |
|---|---|---|---|---|
| **$TeO_2$ [14]** | 4 | 2 | 1.98 | 219 |
| **$La_2O_3$ [36]** | 7 | 5 | 2.53 | 144.06 |
| **$TiO_2$[14]** | 6 | 4 | 1.96 | 226 |

*Table 5. The values of average ring size (l), average cross-link density ($\overline{n}_c$), average stretching force constant ($\overline{F}_a$), theoretical bulk modulus ($K_{bc}$), ratio $K_{bc}$ / $K_e$, and number of network bond per unit volume, ($n_b$) of (95-x) $TeO_2$-5$La_2O_3$-x$TiO_2$ glass system.*

| $x$ (mol %) | $l$ ±0.003 | $\overline{n}_c$ | $\overline{F}_a$ ($Nm^{-1}$) | $K_{bc}$(GPa) ±0.10 | $K_{bc}/K_e$ ±0.04 | $n_b$ x10$^{28}$(m$^{-3}$) ±0.02 |
|---|---|---|---|---|---|---|
| **0** | 0.485 | 2.29 | 212 | 79.39 | 2.19 | 8.27 |
| **5** | 0.484 | 2.38 | 213 | 82.81 | 2.26 | 8.62 |
| **10** | 0.482 | 2.48 | 214 | 86.19 | 2.29 | 8.97 |
| **15** | 0.479 | 2.57 | 215 | 89.39 | 2.32 | 9.29 |
| **20** | 0.469 | 2.67 | 215 | 93.38 | 2.23 | 9.70 |

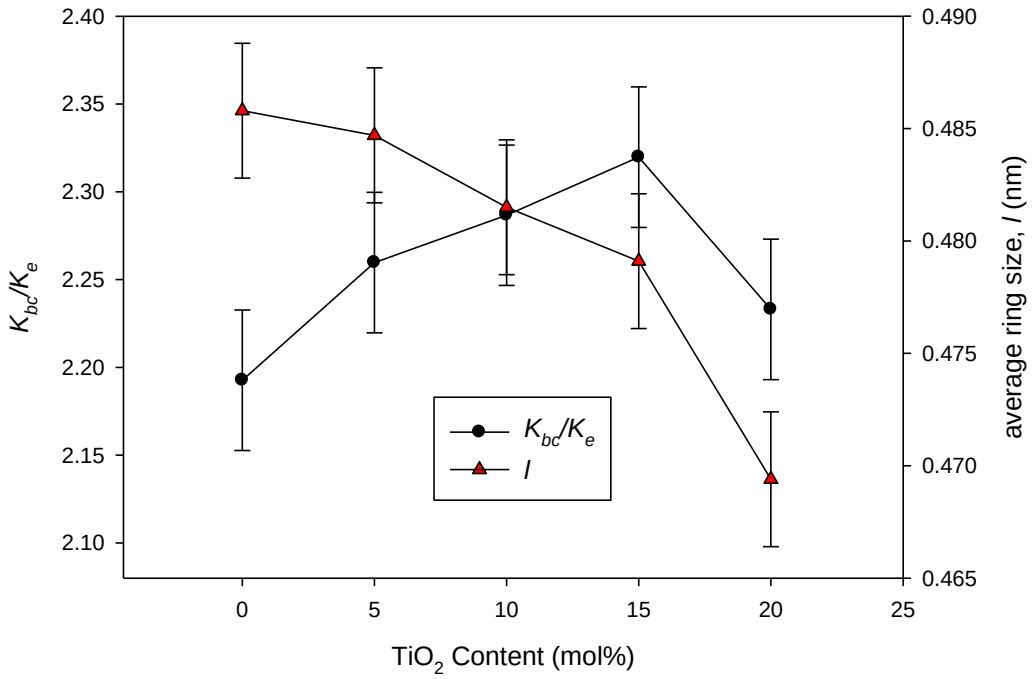


*Fig.11. $K_{bc}/K_e$ ratio and average atomic ring size (l) of (95-x)$TeO_2$-5$La_2O_3$-x$TiO_2$ glass system*

## 4. Discussion

Density is an effective tool to indicate structural compactness [37]. The increase or decrease of density ($\rho$), can be due to either change in molecular mass ($M$), or molar volume ($V_a$). Generally, it is expected that the density and the molar volume should show opposite behavior to each other. However, our present study shows that as $TiO_2$ content is increased, both $\rho$ and $V_a$ decreased (Fig. 2). The decrease in $\rho$ suggests that it is not dominated by the decreasing in $V_a$ but by the large reduction in $M$ due to the smaller atomic mass of $TiO_2$ (molecular mass, 79.87g/mol$^{-1}$) compared to$TeO_2$ (molecular mass, 159.60 g/mol$^{-1}$) of the glass system. Moreover, previous study on $x$$TiO_2$-95$TeO_2$ [38] and 5$Bi_2O_3$-$x$$TiO_2$-(90-$x$)$TeO_2$ [18] also show that the decrease in density was suggested to be correlated with the addition of the relatively lightweight atoms of titanium.

Our suggestion for the increase in rigidity with addition of $TiO_2$ is due to structural modification as evidenced by FTIR results (Fig.3). FTIR analyses which showed shift in absorption peaks assigned to $TiO_4$ from 844 to 866 cm$^{-1}$ indicate increase in BO [22, 39] which was found to be more dominant than NBO with addition of $TiO_2$. Moreover, the increase in the value of $T_g$ can be interpreted to support the increase in rigidity of the glass system. The glass stability $\Delta T$ showed an increasing behaviour and among the glass samples, the 75$TeO_2$-5$La_2O_3$-20$TiO_2$ sample displayed the highest thermal stability which indicates that strongest resistance against thermal shocks [40].

On the other hand, the behaviour of both longitudinal, $v_L$ and shear velocity, $v_s$ in the glass system can be due either change in density ($\rho$) or change in independent moduli ($C_L$ and $\mu$) according to Eq. (2) and (3). In the present study, the increase in both $v_L$ and $v_s$ is suggested to be due to both the decrease in $\rho$ (Figs. 2) and the increase in $C_L$ and $\mu$ (Figs. 7) with addition of $TiO_2$. However, since the behaviour of $v_L$ and $v_s$ (Figs. 6) are quite similar to $C_L$ and $\mu$ (Figs. 7), it gives insight that the velocities were much more dominated by the increase in $C_L$ and $\mu$. Meanwhile, the increase in $C_L$ and $\mu$ indicates increase in stiffness and rigidity respectively of the glass system (Figs. 7). The obvious increase in both $C_L$ and $\mu$ at $x$ = 20 mol% indicates larger improvement in stiffness and rigidity of the glass samples with addition of $TiO_2$. In addition, the increases may also be due to formation of stronger glass network which is attributed to stronger bond strength of Ti-O bond (305 kJ/Mol ) in comparison to Te-O bond (285 kJ/Mol) [41].

Bulk modulus ($K_e$), is a measure of resistance of a material to uniform compression [33]. The steady increase of $K_e$ as shown in Fig. 8 for $x \leq$ 15 mol% with addition of $TiO_2$ indicates a decrease in compressibility. However, at $x$ = 20 mol%, addition of the larger amount of $TiO_2$ seems to cause a much larger decrease in compressibility. Meanwhile, the increase in the Young's modulus ($E$) indicates increasing stiffness of the glass system with the addition of $TiO_2$.

Poisson's ratio, $\sigma$ is defined as the ratio between lateral and longitudinal strain produced when tensile force is applied [10] and it practically decrease with increasing cross-link density and vice versa [10, 14, 34]. Our present results show that $\sigma$ decreased gradually for $x \leq$ 15mol% of $TiO_2$ followed by a larger decrease at $x$ = 20 mol% of $TiO_2$ (Fig. 9) indicating that the actual crosslink density increased gradually for $x \leq$ 15 mol% before a larger increase at $x$ = 20 mol%. This supports our suggestion that $TiO_2$ acts as network former in the glass system. On the other hand, the increase in hardness, $H$ (Fig. 9) indicates the increase in stress required to eliminate free volume in the glass [14]. The large increase in $H$, at $x$= 20 mol% with addition of $TiO_2$ follows from the slight surge in overall rigidity and stiffness of the glass network.

Debye temperature, $\theta_D$ represent the temperature where all modes of vibration in solids are excited [42] and an increasing $\theta_D$ usually implies an increase in the rigidity of the glass. In this study $\theta_D$ may be affected by $V_a$ and $v_m$. However, as illustrated in Fig. 10, since the behavior of $v_m$ is closely similar to that of $\theta_D$ therefore, it can be concluded that the changes in $\theta_D$ is dominated by the value of $v_m$. Futhermore, as $v_m$ depends on $v_L$ and $v_s$, thus, the change in $\theta_D$ correctly reflects the change in rigidity and stiffness of the glass system [17, 32, 33].

Theoretical bulk modulus, $K_{bc}$ of the glass system was calculated using the bulk compression model and it is found to be consistently higher than $K_e$ values (Fig. 11) which indicates that the actual compression mechanism is slightly different from the ideal compression mechanism [42]. The increase in the $K_{bc}$values is related to the replacement of the tellurium atoms with coordination number $n_f$ = 4 and ideal crosslink density per cation $n_c$ = 2 by the transition

metal titanium atoms which has a coordination number $n_f$ = 6 and ideal crosslink density percation $n_c$= 4 (Table 4). The values of the ratio $K_{bc}/K_e$ gradually increased from 2.19 to 2.32 for $x \leq 15$ mol% before a sudden drop to 2.23 at $x$ = 20 mol% with addition of $TiO_2$. This indicates for $x \leq 15$ mol%, increase in non-isotropic compression and some other mechanism took place such as ring deformation or bending [16, 17, 32]. However, the decrease in $K_{bc}/K_e$ at $x$ = 20 mol% indicates ring deformation or bending was reduced with addition of $TiO_2$. On the other hand, the average atomic ring size, $l$ tend to decrease from 0.485 nm to 0.469 nm indicating stronger influence of $l$ on $K_e$ as expressed by Eq. (11) Thus, the decreasing of $l$ indicates stiffening of the glass [10]. However, our $K_{bc}/K_e$ value of around 2 suggests that although there were some deformations or bending taking place during compression, the main compression mechanism was still mainly isotropic ring compression.

## 5. Conclusions

Effects of concurrent addition of $TiO_2$ and reduction of $TeO_2$ on elastic, strcture and thermal properties of (95-$x$)$TeO_2$-5$La_2O_3$-$x$$TiO_2$ ($x$ = 0, 5, 10, 15, 20 mol %) lanthanum tellurite glass system have been studied**.** Independent elastic moduli, $C_L$ and $\mu$ and related elastic moduli and the Debye temperature, $\theta_D$ were observed to increase with substitution of $TiO_2$ from $x$ = 0to $x$ = 20 mol% indicating increase in stiffness and rigidity of glass system. Our results were supported by FTIR analyses which showed increase of BO which enhanced network lingkage and DSC analysis which showed increase in the glass transition temperature, $T_g$. The results suggests the role of $TiO_2$ as a network former. Our analysis using bulk compression and ring deformation models revealed that $K_{bc}/K_e$ ratio increased from 2.19 ($x$ = 0 mol%) to 2.32 ($x$ = 15 mol%) indicating slight increase in ring deformation or bending upon compression with addition of $TiO_2$. However, the decrease in $K_{bc}/K_e$ at $x$ = 20 mol% indicates a reverse effect.

**Acknowledgement**

Financial support by the Ministry of Education of Malaysia under the FRGS grant (RMI, UiTM-(600-RMI/FRGS 5/3 (55/2014)) is gratefully acknowledged.

## References

[1] R.El-Mallawany, L.M.Sharaf El-Deen, M.M.Elkholy, J. of Mater. Sci.**31,** 6339(1996).
[2] M.M.Ahmad, E.S.Yousef, E.S.Moustafa, Physica B: Condensed Matter **371,** 74 (2006).
[3] M.P.Kumar, T.Sankarappa, B.V.Kumar, N.Nagaraja, Solid State Sciences, **11,** 214 (2009).
[4] R.El-Mallawany, M.D. Abdalla, I.A. Ahmed, Mater. Chem. Phys. **109**, 291 (2008).
[5] G.Upender, V.C.Mouli, Journal of Molecular Structure, **1006,** 159 (2011).
[6] A.G.Kalampounias, G.N.Papatheodorou, S.N. Yannopoulos, J.Phys Chem. Solids, **67,** 72(2006).
[7] A.A.El-Moneim, Mater. Chem. Phys. **73,** 318 (2002).
[8] J.Lin, W.Huang, Z.Sun, C.S.Ray, D.E.Day, J.Non-Cryst. Solids, **336**, 189 (2004).
[9] Y.B.Saddeek, H.A.Afifi, N.S.Abd El-Aal, Physica B: Condensed Matter, **398**, 1 (2007).
[10] M.A.Sidkey, R.El-Mallawany, R.I.Nakhlaal, A.Abd El.Moneim, J. Non-Cryst. Solids, **215**, 75 (1997).
[11] G.Upender, S.Ramesh, M.Prasada, V.G.Satheb,V.C.Moulia, J.Alloys Compd **504**, 468 (2010).
[12] Ikushima, J.Akira, J. Non-Cryst. Solids, **178**, 1 (1994).
[13] Wang, J.S., E.M.Vogel, E.Snitzer, Optical Materials, **3,** 187 (1994).
[14] R.El-Mallawany, N.El-Khoshkhany, H.A.Afifi, Mater. Chem. Phys. **95**, 321 (2006).
[15] N.B.Mohamed, A. K.Yahya, M. S. M.Deni, S. N.Mohamed, M. K.Halimah, H. A. A.Sidek, J. Non-Cryst. Solids, **356**, 1626 (2010).

[16] S.Azianty, A.K. Yahya, M.K. Halimah, J. Non-Cryst. Solids, **358,** 1562 (2012).
[17] M.M.Umair, A.K. Yahya, Mater. Chem. Phys. **142**, 549 (2013).
[18] M.Udovica, P.Thomasa, A.Mirgorodskya, O.Duranda, M.Soulisa, O.Massona, T.M.Mejeana, J.C.C.Mesjarda, J. Solid State Chem. **179**, 3252 (2006).
[19] T.A.Mohamed, I.Shaltout, K.M.Al Yahyaei, Spectrochim Acta A Mol Biomol Spectrosc **64**, 106 (2006).
[20] J.C.Sabadel, P.Armand, D.C.Herreillat, P.Baldeck, O.Doclot, A.Ibanez, E.Philippot, J.Solid State Chem. **132**, 411 (1997).
[21] F.Chen, T. Xu, S.Dai, Q .Nie, X .Shen, J .Zhang, X .Wang, Optical Materials **32**, 868 (2010).
[22] W.Stambouli, H.Elhouichet, M.Ferid, Journal of Molecular Structure, **1028**, 39(2012).
[23] L.Barbieri, A.B.Corradi, C.Leonelli, C.Siligardi, T.Manfredini, G.C.Pellacani, J.Appl. Phys, **81**, 1481(1997).
[24] Sekiya, T.Mochida, N.Ohtsuka, A.Tonokawa, Mamoru, J.Non-Cryst. Solids, **144,** 128 (1992).
[25] A.Berthereau, Y.Le Luyer, R Olazcuaga,G.Le Flem, M.Couzi, L.Canioni,P.Segonds, L.Sarger, A.Ducasse, Materials Research Bulletin, **29**, 933 (1994).
[26] V. V.Dorofeev,A. N Moiseev,M. F.Churbanov, G. E.Snopatin, A. V.Chilyasov, I. A Kraev,.A. S.Lobanov,T. V.Kotereva, L. A.Ketkova, A. A.Pushkin, V. V.Gerasimenko, V. G.Plotnichenko, A. F.Kosolapov, E. M.Dianov, Optical Materials, **33**, 1911 (2011).
[27] M.R. Oermann,H.E.Heidepriem, Y.Li, T.C.Foo, T.M. Monro, Optical Society of America, **17**,(2009).
[28] M.S.Gaafar, H.A.Afifi, M.M. Mekawy, Physica B: Condensed Matter, **404**, 1668 (2009).
[29] M.S.Gaafar, Y.B. Saddeek, L. Abd El-Latif, J.Phys Chem. Solids, **70**, 173 (2009).
[30] A.V.G.Devi,V.Rajendran,N.Rajendran, Journal of Engineering Science and Technology **2**, 2483 (2010).
[31] M.S.Sidkey, J.Non-Cryst. Solids, **215**, 75 (1997).
[32] S.Azianty,A.K. Yahya, J.Non-Cryst. Solids, **378**, 234 (2013).
[33] S.Laila, S.N.Supardan, A.K.Yahya, J.Non-Cryst. Solids, **367**, 14 (2013).
[34] N.Baizura,A.K. Yahya, J.Non-Cryst. Solids, **357**, 2810 (2011).
[35] R. El-Mallawany, CRC Press,New York, 2002.
[36] Y.B.Saddeek, Glass Physics and Chemistry, **38**, 373 (2012).
[37] L.Barbieri, A.B.Corradi, C. Leonelli, C.Siligardi, T.Manfredini, G.C.Pellacani Material Reserch Bulletin, **32**, 637 (1997).
[38] V.Dimitrov,T.Komatsu, J.Non-Cryst. Solids, **249**, 160 (1999).
[39] B. V.Raghavaiah, C.Laxmikanth, N.Veeraiah, Optics Communications, **235**, 341 (2004).
[40] R.El-Mallawany, J.Non-Cryst. Solids, **379**, 177 (2013).
[41] V. Dimitrov, T.Komatsu , Journal of the University of Chemical Technology and Metallurgy, **45,** 219(2010).
[42] H.A.Afifi, S. Marzouk, Mater. Chem. Phys. **80**, 517 (2003).